Electronic Supplementary Material (ESI) for Organic & Biomolecular Chemistry.

Solvent effects on the folding of *ortho*-phenylene oligomers

Supporting Information

*Gopi Nath Vemuri, Meng Chu, Han Dong, Brian J. Spinello, and C. Scott Hartley**

Department of Chemistry & Biochemistry, Miami University, Oxford, OH 45056, USA

Table of Contents

List of Figures

List of Schemes

List of Tables

Supplementary Figures

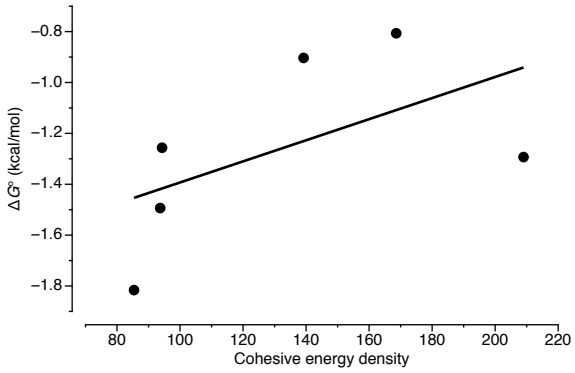

Figure S1. Plot of experimental $\Delta G^{\circ}_{\mathrm{AAB}}$ vs solvent cohesive energy density ($R^2 = 0.31$).

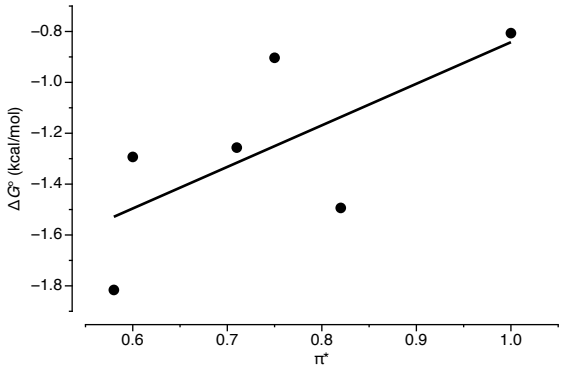

Figure S2. Plot of experimental $\Delta G^{\circ}_{\mathrm{AAB}}$ vs solvent π^* ($R^2 = 0.46$).

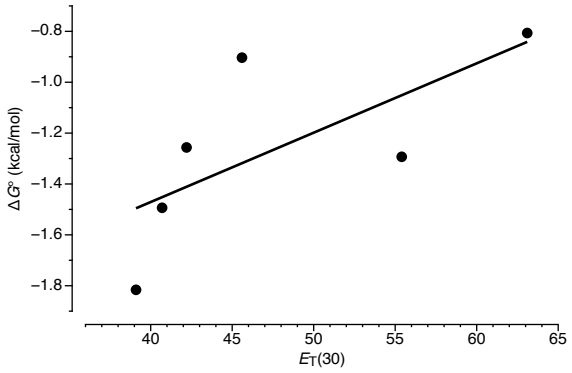

Figure S3. Plot of experimental $\Delta G^{\circ}_{\mathrm{AAB}}$ vs solvent $E_T(30)$ ($R^2 = 0.48$).

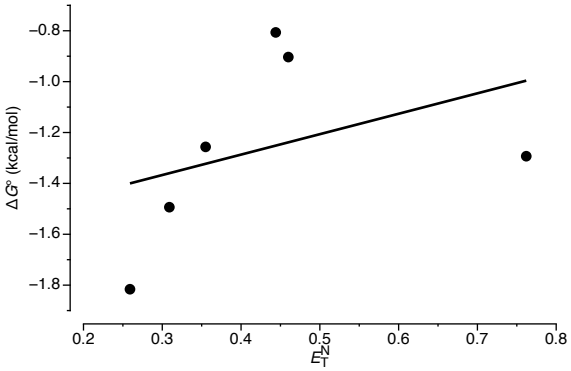

Figure S4. Plot of experimental $\Delta G^{\circ}_{\mathrm{AAB}}$ vs solvent E_T^N ($R^2 = 0.15$).

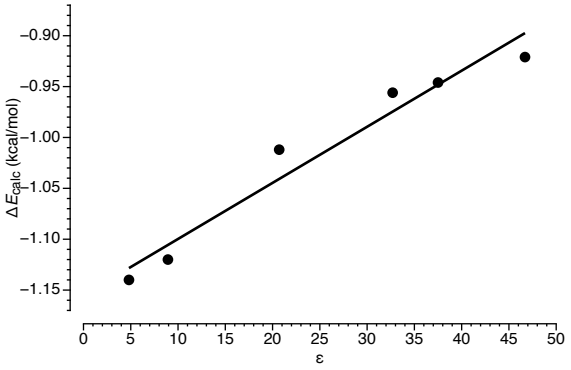

Figure S5. Plot of experimental ΔE_{calc} vs solvent ε ($R^2 = 0.95$).

Solvent studies on methoxy-substituted hexamer oP^6(OMe)

To confirm that the trend of worsened folding with increasing solvent dielectric holds for other *o*-phenylene systems, we carried out a similar solvent-dependence study on methoxy-substituted hexamer **oP^6(OMe)**. NMR analysis of this system has been previously reported.[1]

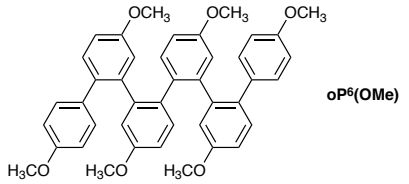

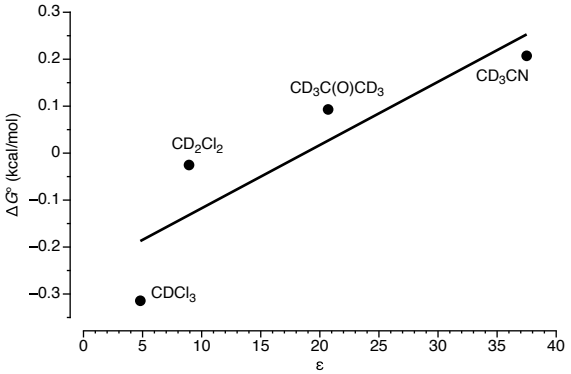

Figure S6. Plot of experimental $\Delta G^{\circ}_{\mathrm{AAB}}$ for methoxy-substituted hexamer **oP^6(OMe)** vs solvent ε (-5 ℃).

Quaternization of oP^6(NMe$_2$) to oP^6(NMe$_3^+$)

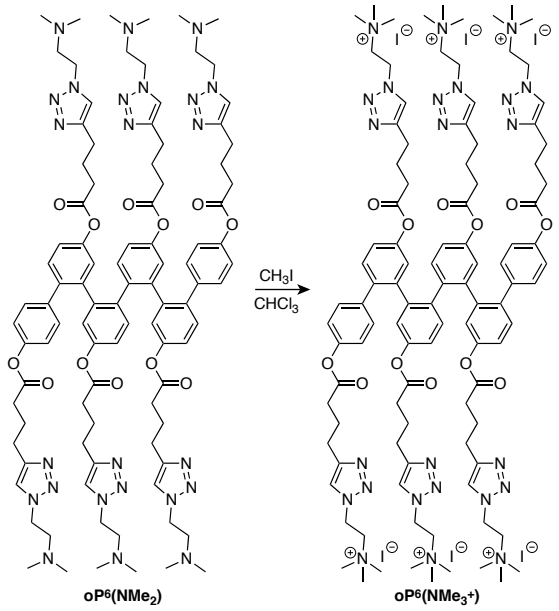

Scheme S1. Quaternization of **oP^6(NMe$_2$)** to give **oP^6(NMe$_3^+$)**.

Compound **oP^6(NMe$_3^+$)** was obtained by methylation of **oP^6(NMe$_2$)**, as follows: CH_3I (0.2 mL) was added to a stirred solution of **oP^6(NMe$_2$)** (8 mg) in $CHCl_3$ (2.0 mL) in a scintillation vial. The reaction mixture was stirred for 16 h at room temperature and concentrated under reduced pressure to afford 14 mg of **oP^6(NMe$_3^+$)** (hexaiodide salt) as a pale yellow semi solid which was used without further purification. ^{1}H NMR (500 MHz, D_2O) δ 8.06–7.90 (m, 6H), 7.22–7.06 (m, 4H), 6.88 (s, 2H), 6.72 (d, J = 7.4 Hz, 6H), 6.54 (d, J = 7.4 Hz, 4H), 6.19 (s, 2H), 6.01 (d, J = 8.0 Hz, 2H), 5.05–4.85 (m, 12H), 4.04–3.86 (m, 12H), 3.21–3.06 (m, 54H), 2.98–2.62 (m, 24H), 2.26–2.01 (m, 12H); HRMS (ESI) calcd for $C_{102}H_{140}N_{24}O_{12}^{6+}$ (M^{6+}) 315.51749, found 315.51755.

The aromatic region of its ^{1}H NMR spectrum (D_2O), shown in Figure S7, suggests that the compound remains well-folded. The full spectrum is shown in S42.

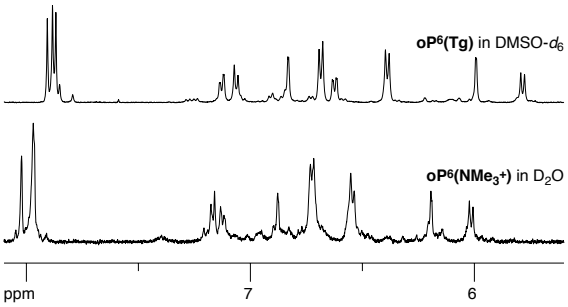

Figure S7. ^{1}H NMR spectrum (500 MHz, D_2O) of **oP^6(NMe$_3^+$)**. The spectrum of **oP^6(Tg)** in DMSO-d_6 is included for comparison.

Computational Data

All energies are for optimized geometries at the PCM/B97-D/TZV(2d,2p) level, calculated using Gaussian 09.[2] Cartesian coordinates are included in a separate file in plain text format.

Solvent	Conformer	Energy (E_h)	ZPC (E_h)	Total Energy (E_h)	IF
$CHCl_3$[3]	AAA	−2753.908338	0.731032	−2753.177306	0
$CHCl_3$[3]	AAB	−2753.906521	0.731787	−2753.174734	0
CH_2Cl_2	AAA	−2753.912215	0.730659	−2753.181556	0
CH_2Cl_2	AAB	−2753.910430	0.731486	−2753.178944	0
$CH_3C(O)CH_3$	AAA	−2753.915039	0.730475	−2753.184564	0
$CH_3C(O)CH_3$	AAB	−2753.913426	0.731358	−2753.182067	0
CH_3OH	AAA	−2753.915919	0.730438	−2753.185481	0
CH_3OH	AAB	−2753.914396	0.731313	−2753.183083	0
CH_3CN	AAA	−2753.916050	0.730430	−2753.185620	0
CH_3CN	AAB	−2753.914543	0.731300	−2753.183242	0
$CH_3S(O)CH_3$	AAA	−2753.916385	0.730391	−2753.185995	0
$CH_3S(O)CH_3$	AAB	−2753.914918	0.731268	−2753.183649	0

Table S1. Computational data for optimized geometries of **oP^6(OAc)**. IF = number of imaginary frequencies.

EXSY Spectra of oP^6(Tg) and oP^{10}(Tg)

EXSY spectra for **oP^6(Tg)** and **oP^{10}(Tg)** in various solvents are shown in Figures S8–S17. Briefly, these experiments confirm that the minor peaks observed in the 1D spectra result from minor conformational states in slow exchange with the major (helically folded) state. They also allow one to determine which signals in the minor conformers correspond to which in the major conformers, which helps select the signals that are integrated to determine the conformational distribution. For this study, the triazole protons were chosen as they were typically well-separated and it is generally easier to deconvolute singlets. For more information, please see our earlier papers on the conformational analysis of *o*-phenylenes.[1,4]

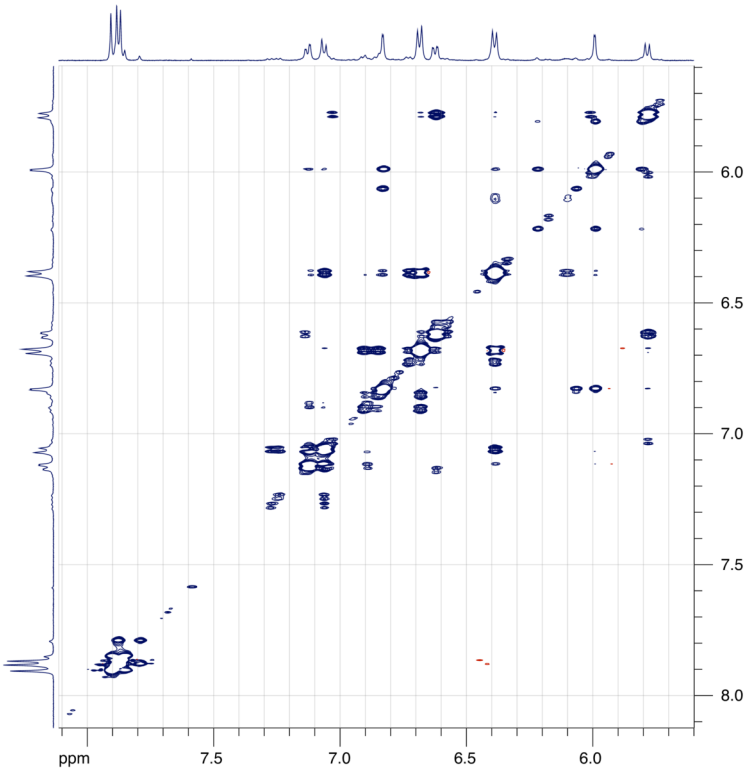

Figure S8. EXSY spectrum (500 MHz, $CD_3S(O)CD_3$) of **oP^6(Tg)**.

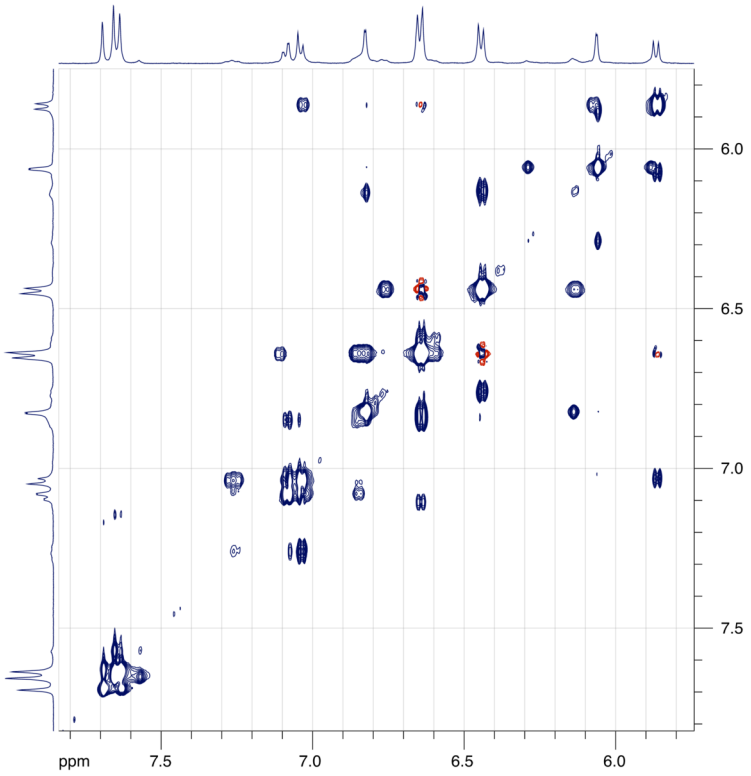

Figure S9. EXSY spectrum (500 MHz, CD_3CN) of **oP^6(Tg)**.

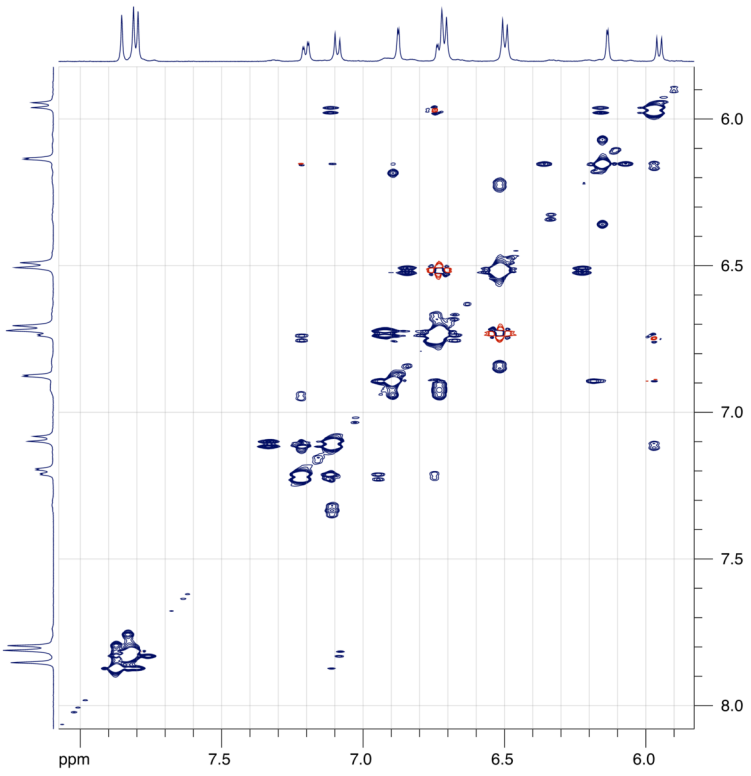

Figure S10. EXSY spectrum (500 MHz, $CD_3C(O)CD_3$) of **oP^6(Tg)**.

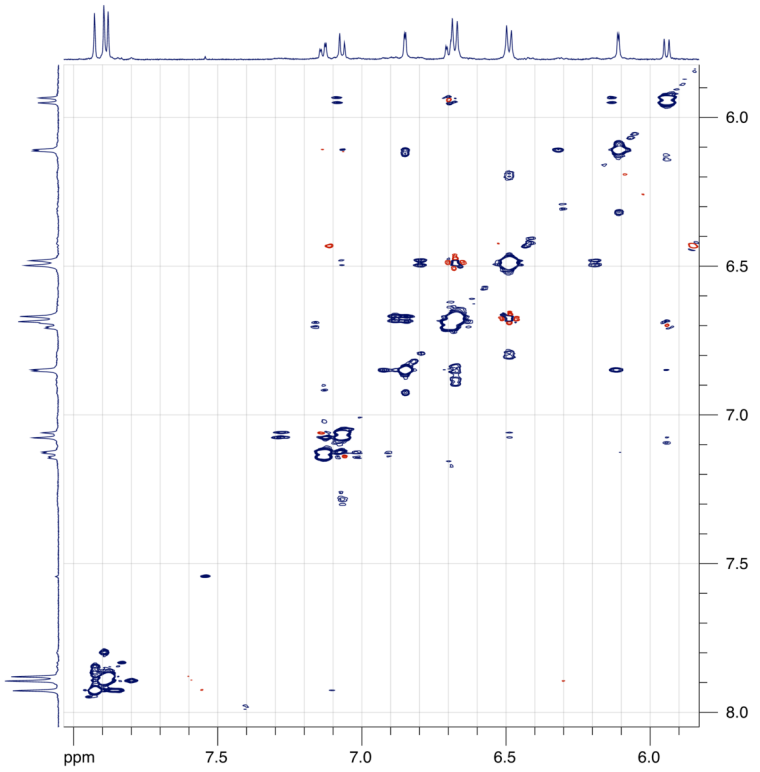

Figure S11. EXSY spectrum (500 MHz, CD_3OD) of **oP^6(Tg)**.

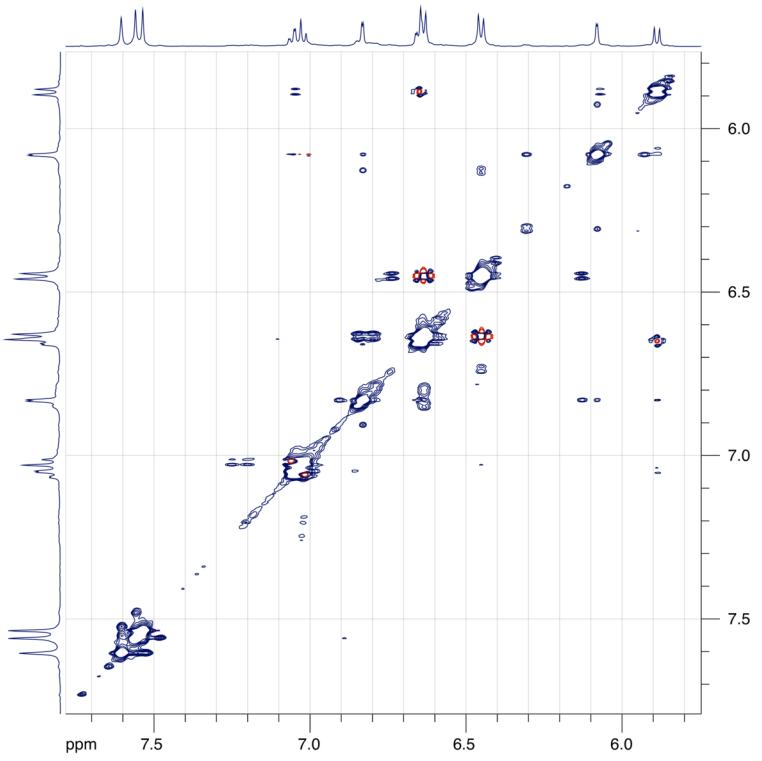

Figure S12. EXSY spectrum (500 MHz, CD_2Cl_2) of **oP^6(Tg)**.

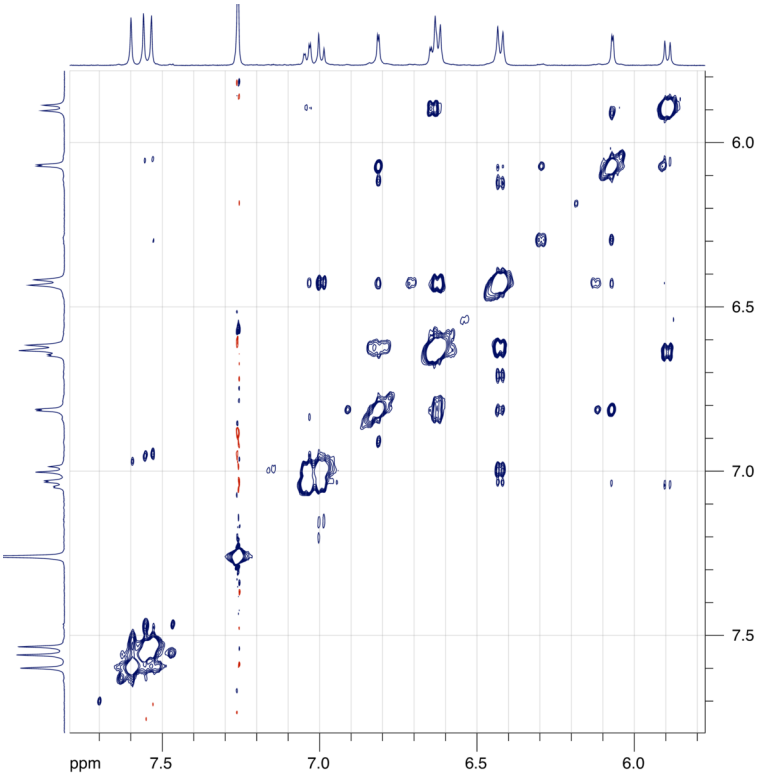

Figure S13. EXSY spectrum (500 MHz, $CDCl_3$) of **oP^6(Tg)**.

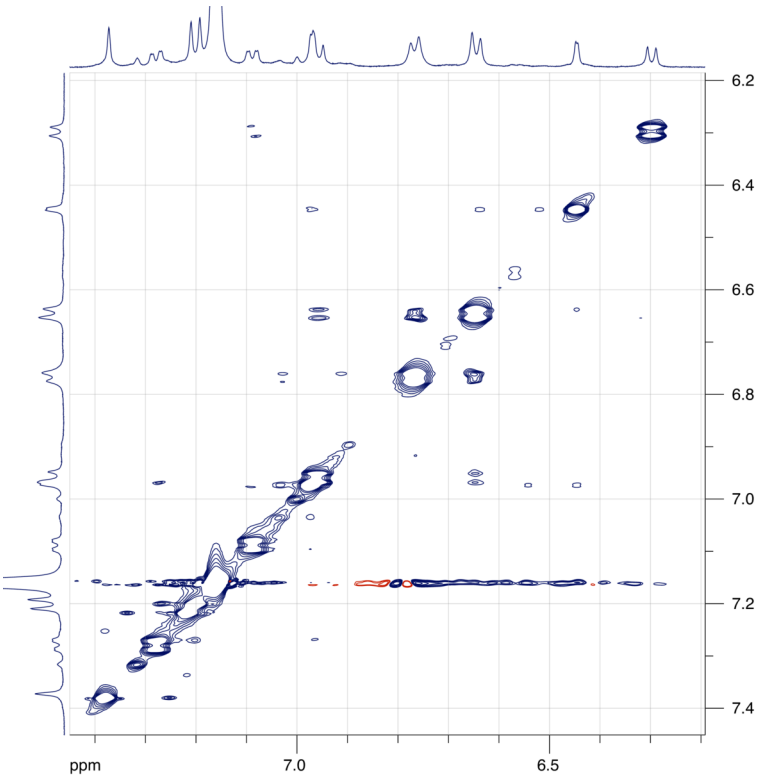

Figure S14. EXSY spectrum (500 MHz, C_6D_6) of **oP^6(Tg)**.

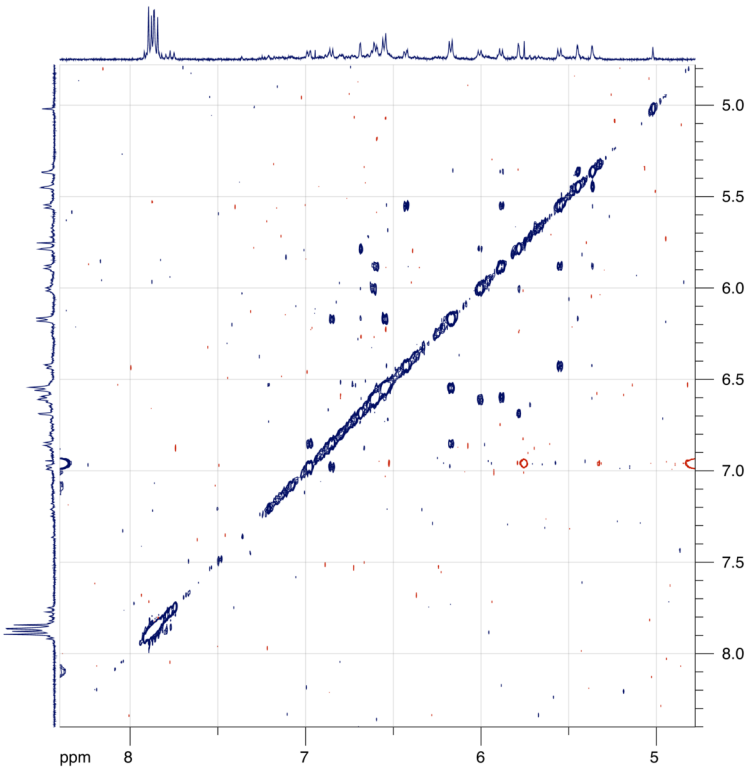

Figure S15. EXSY spectrum (500 MHz, $CD_3S(O)CD_3$) of **oP^{10}(Tg)**.

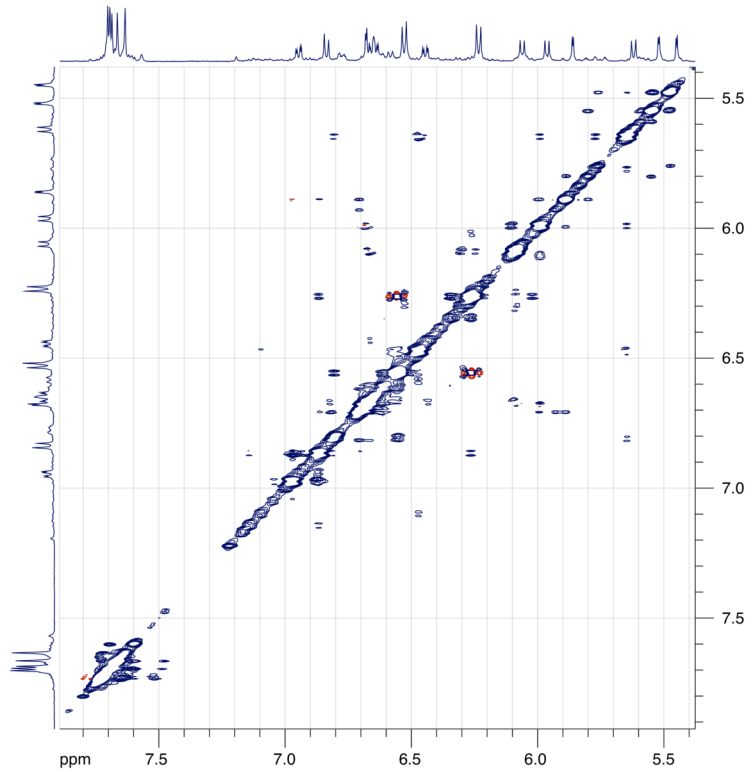

Figure S16. EXSY spectrum (500 MHz, CD_3CN) of **oP^{10}(Tg)**.

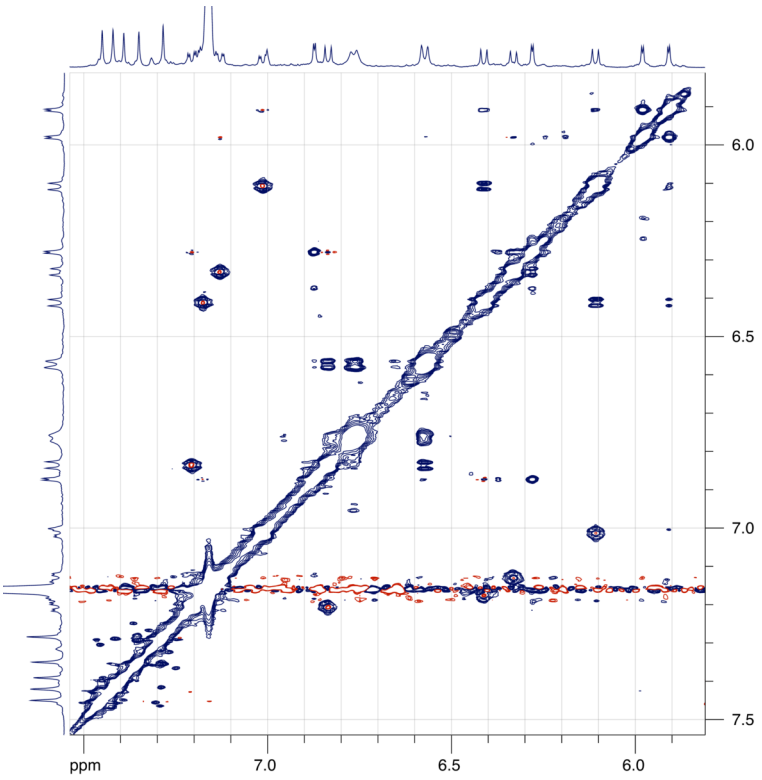

Figure S17. EXSY spectrum (500 MHz, C_6D_6) of **oP^{10}(Tg)**.

^{1}H and ^{13}C NMR Spectra

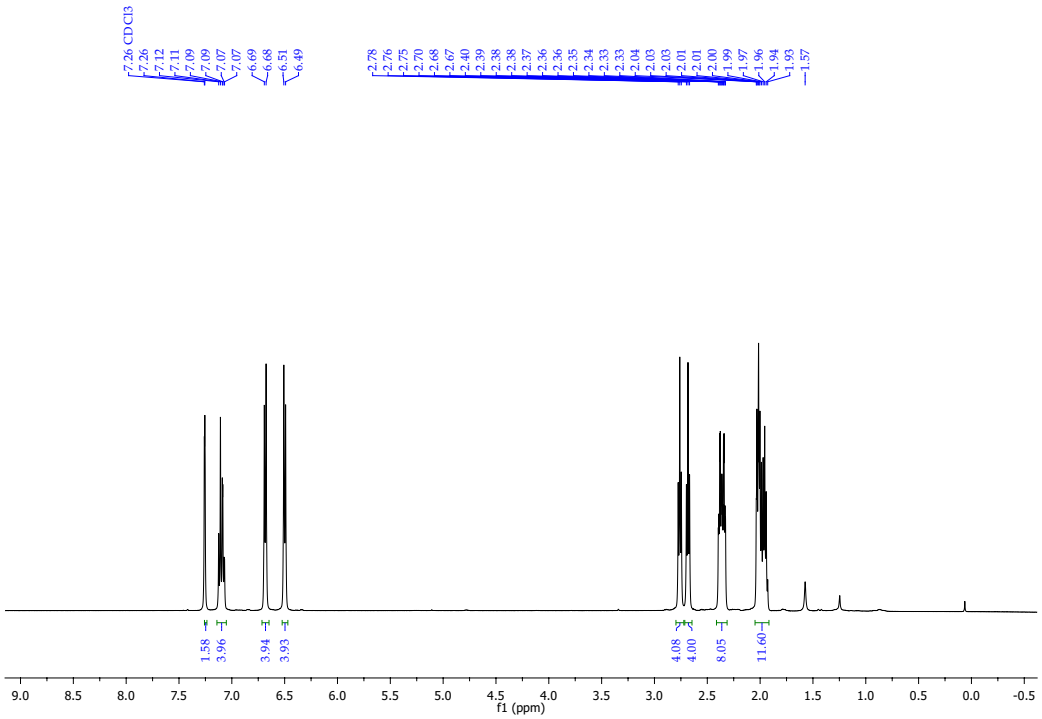

Figure S18. ^{1}H NMR spectrum (500 MHz, $CDCl_3$) of **2**[4].

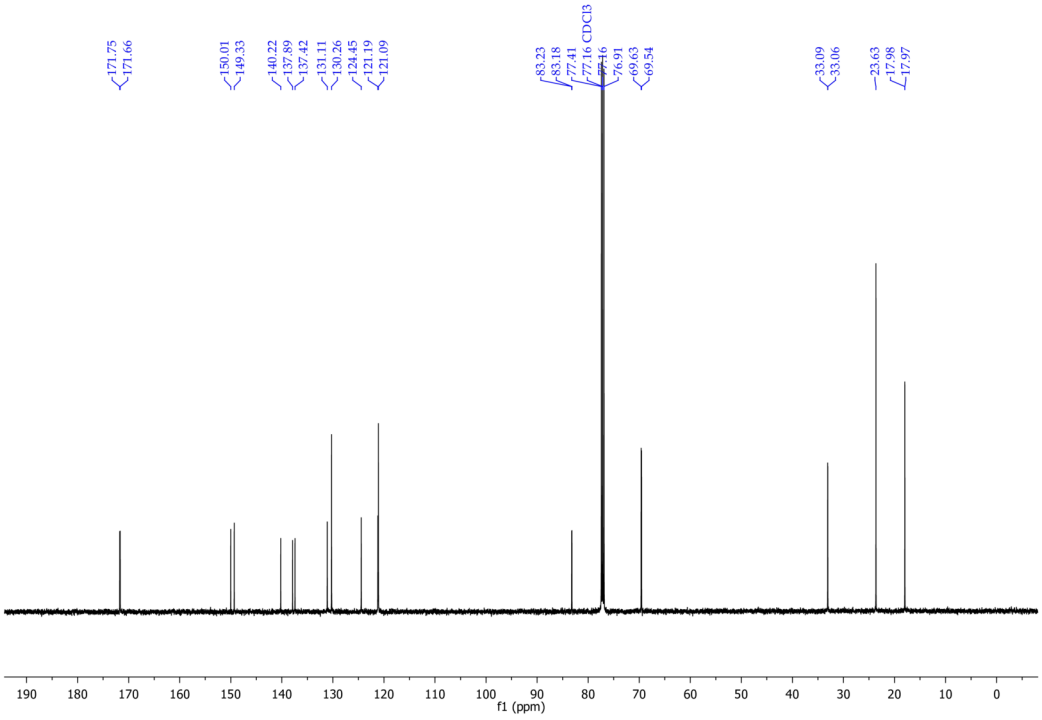

Figure S19. ^{13}C NMR spectrum (125 MHz, $CDCl_3$) of **2**[4].

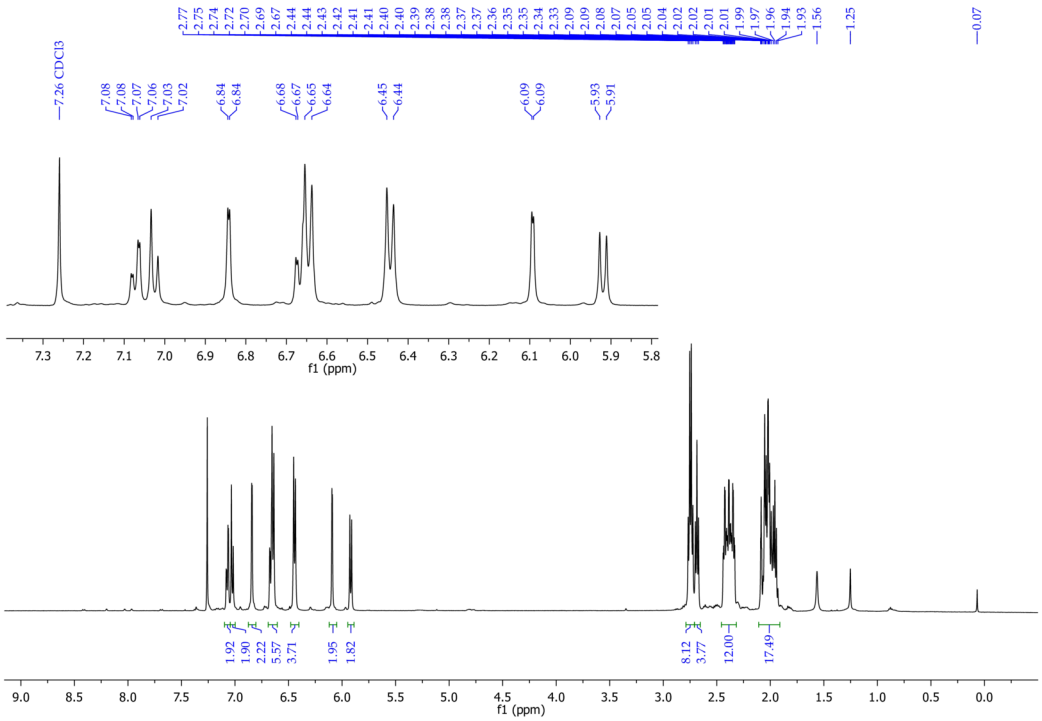

Figure S20. ^{1}H NMR spectrum (500 MHz, $CDCl_3$) of **2**^{6}.

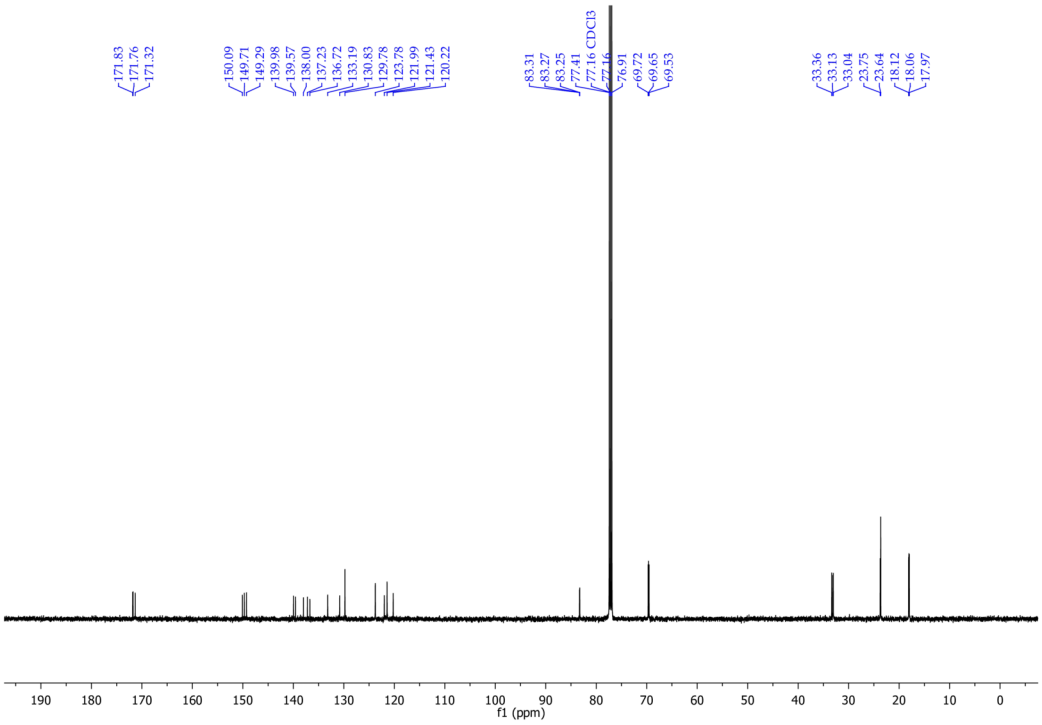

Figure S21. ^{13}C NMR spectrum (125 MHz, $CDCl_3$) of **2**^{6}.

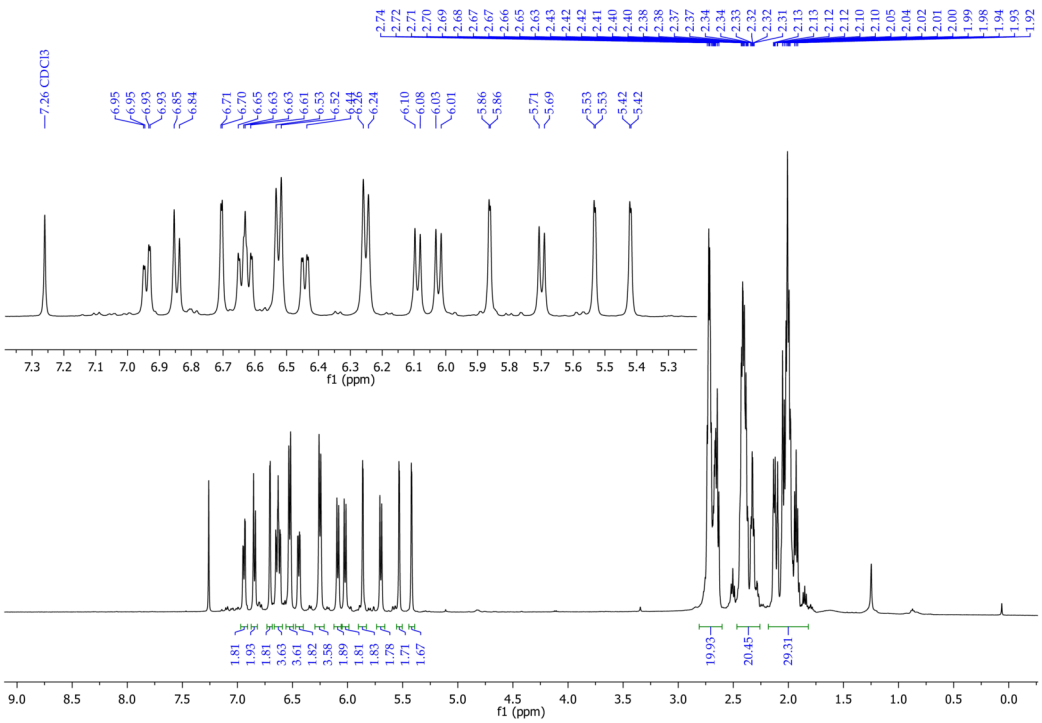

Figure S22. ^{1}H NMR spectrum (500 MHz, $CDCl_3$) of **2**[10].

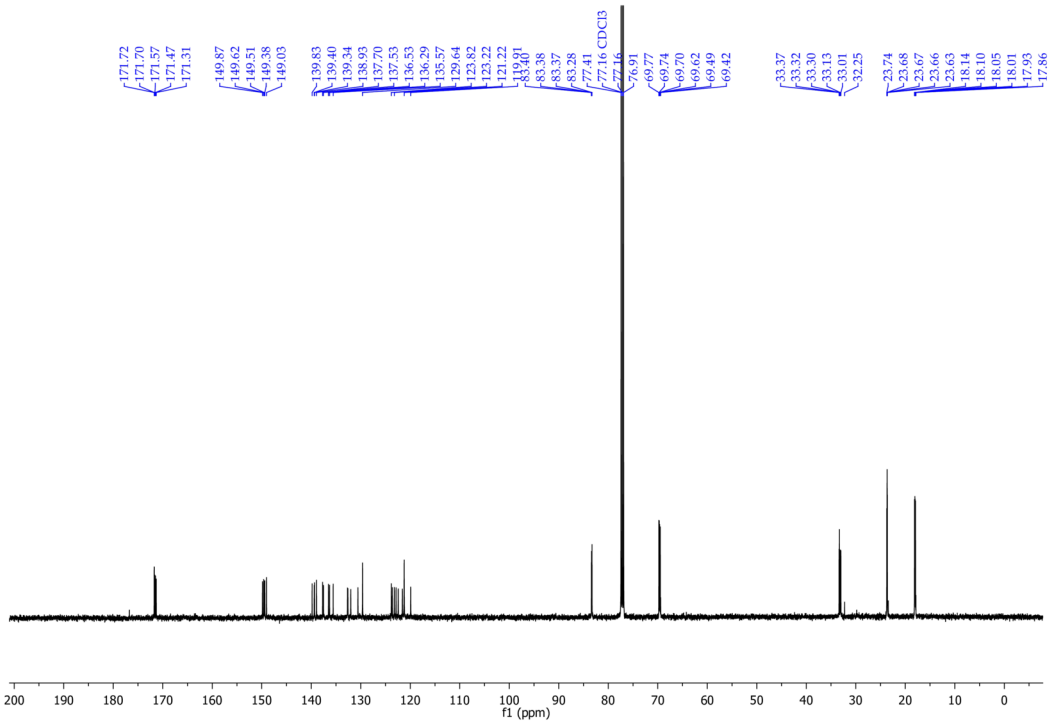

Figure S23. ^{13}C NMR spectrum (125 MHz, $CDCl_3$) of **2**[10].

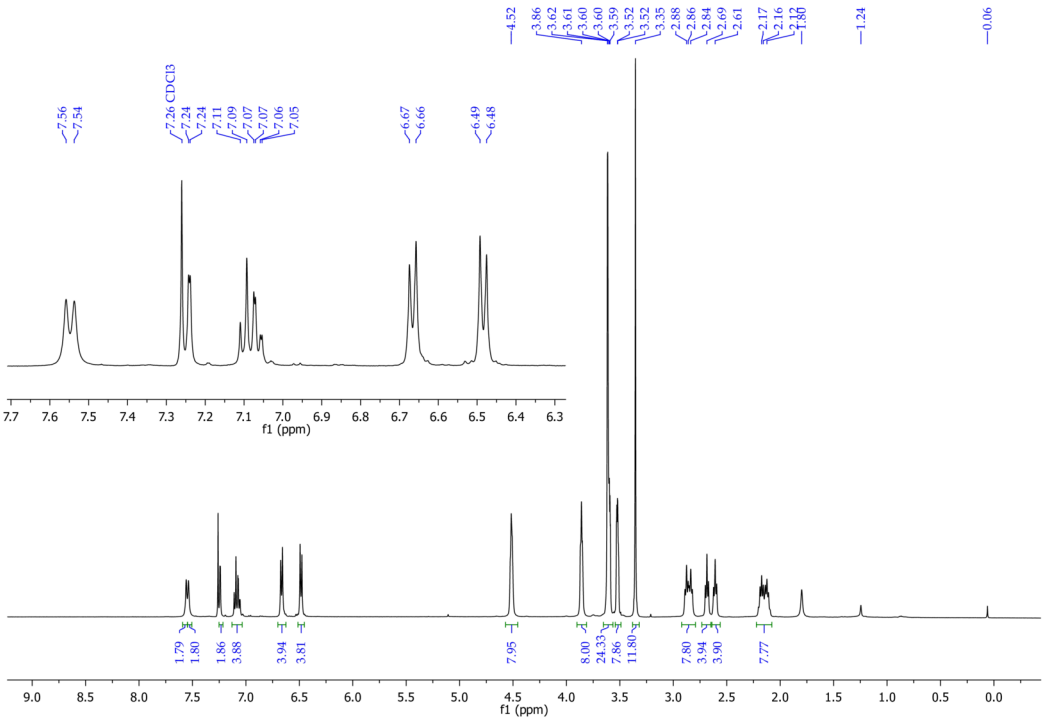

Figure S24. ^{1}H NMR spectrum (500 MHz, $CDCl_3$) of **oP^4(Tg)**.

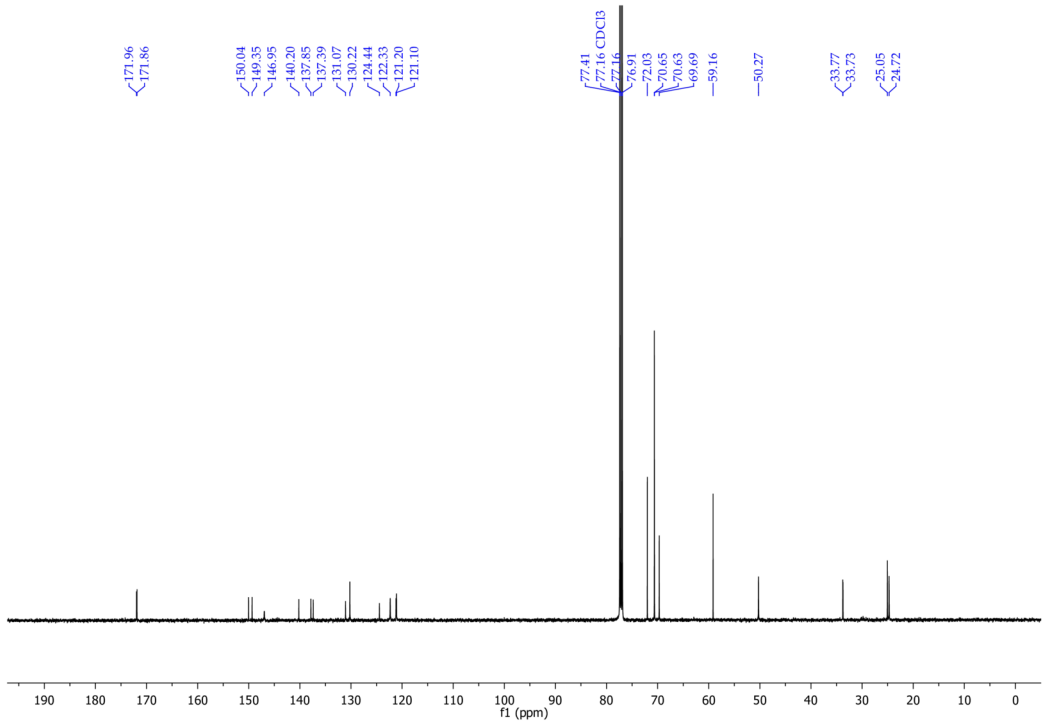

Figure S25. ^{13}C NMR spectrum (125 MHz, $CDCl_3$) of **oP^4(Tg)**.

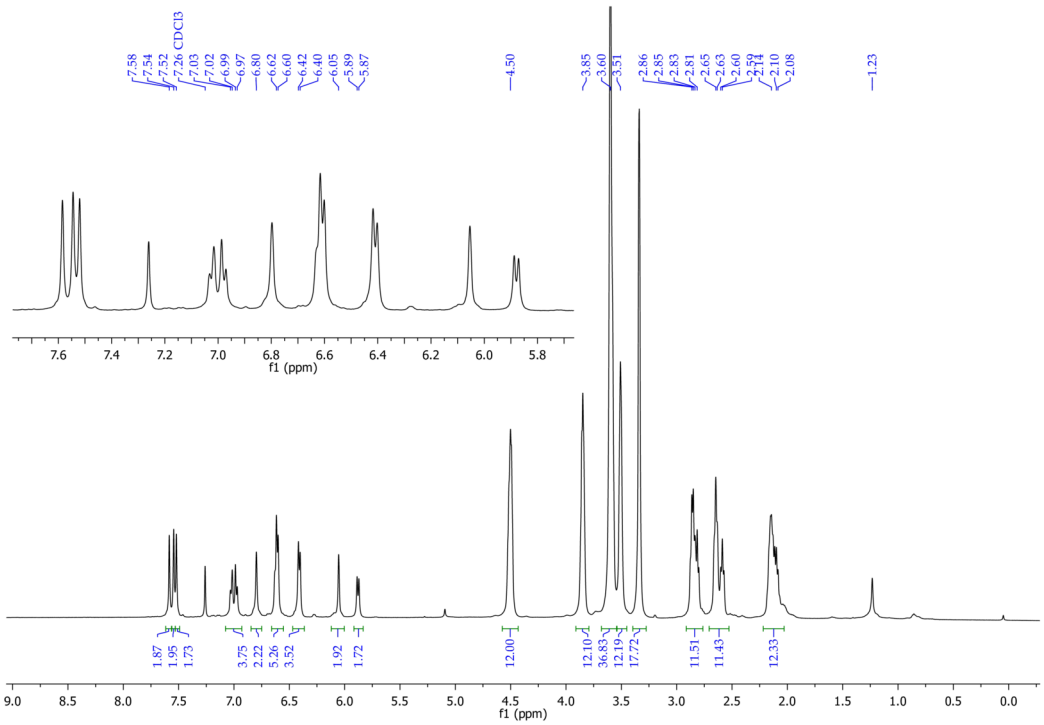

Figure S26. ^{1}H NMR spectrum (500 MHz, $CDCl_3$) of **oP^6(Tg)**.

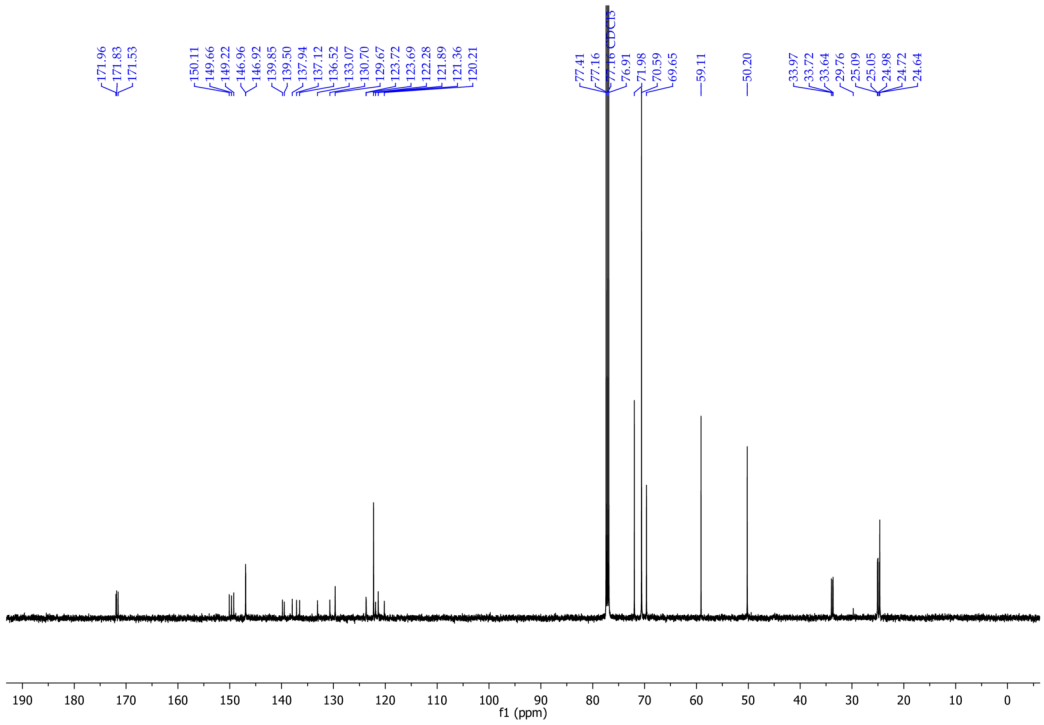

Figure S27. ^{13}C NMR spectrum (125 MHz, $CDCl_3$) of **oP^6(Tg)**.

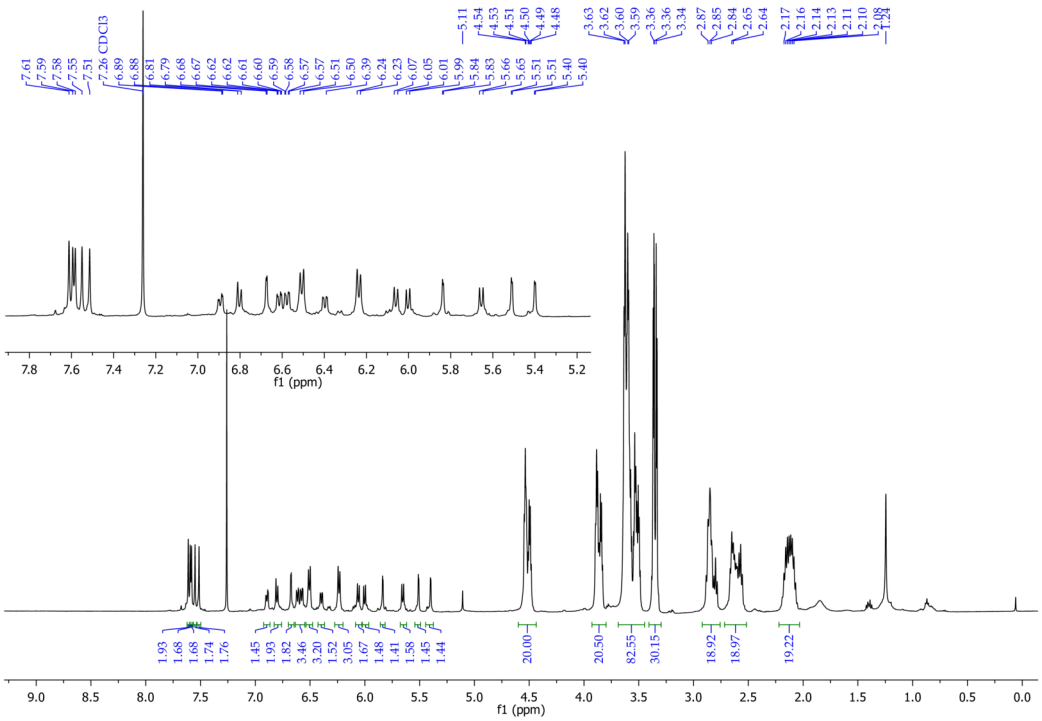

Figure S28. ^{1}H NMR spectrum (500 MHz, $CDCl_3$) of **oP^{10}(Tg)**.

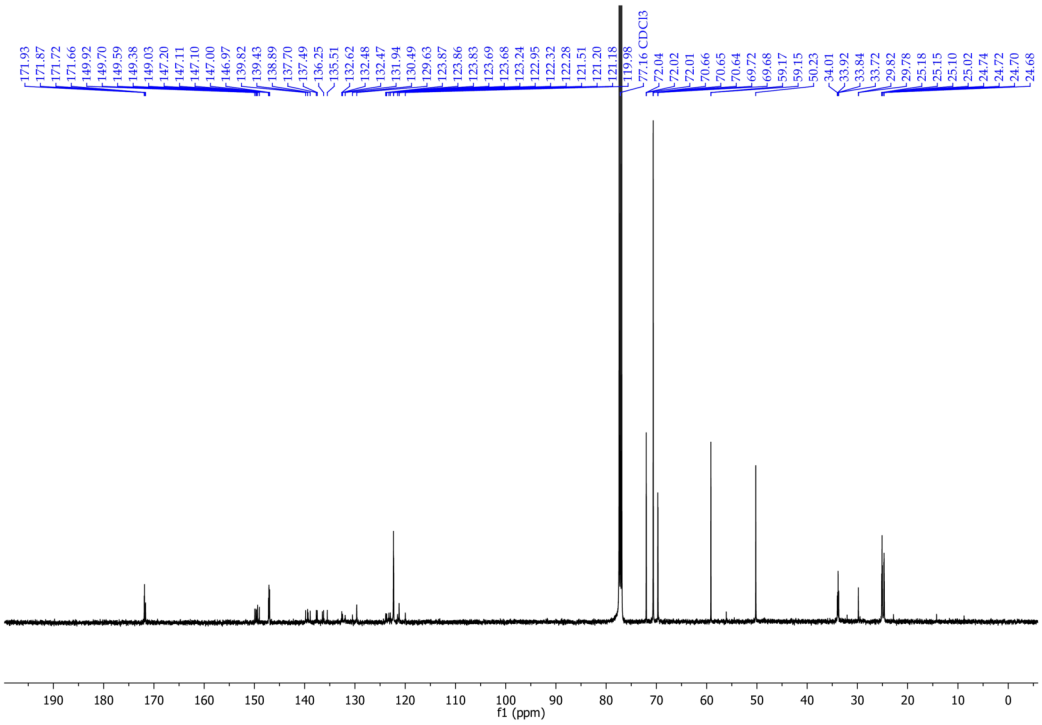

Figure S29. ^{13}C NMR spectrum (125 MHz, $CDCl_3$) of **oP^{10}(Tg)**.

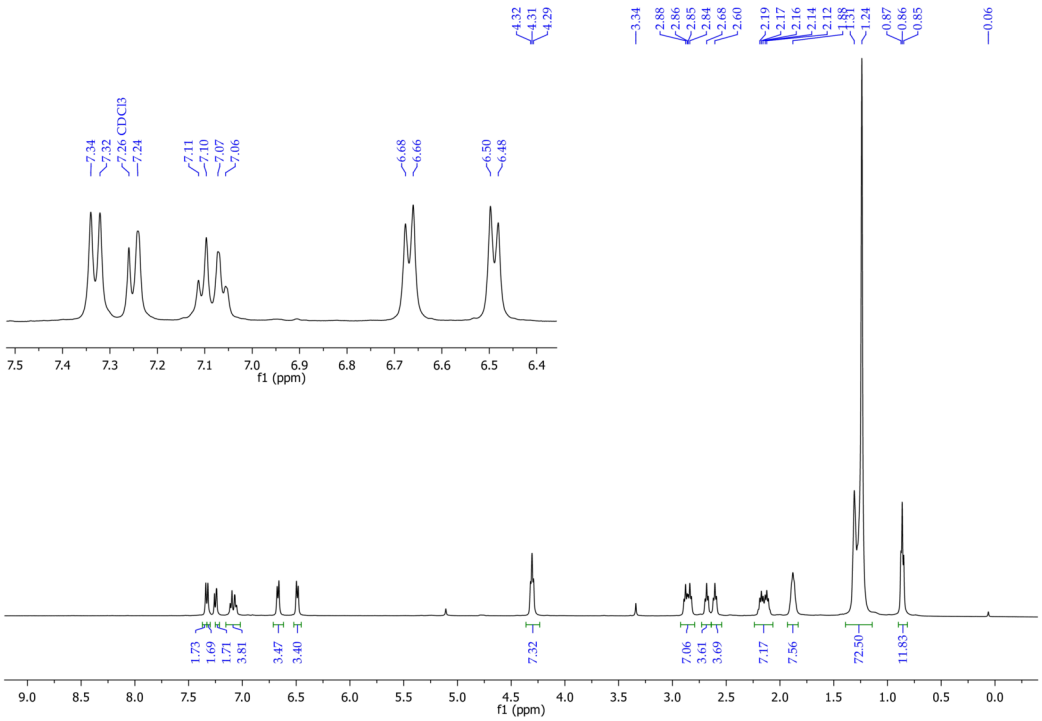

Figure S30. ^{1}H NMR spectrum (500 MHz, $CDCl_3$) of **oP^4(C_{12})**.

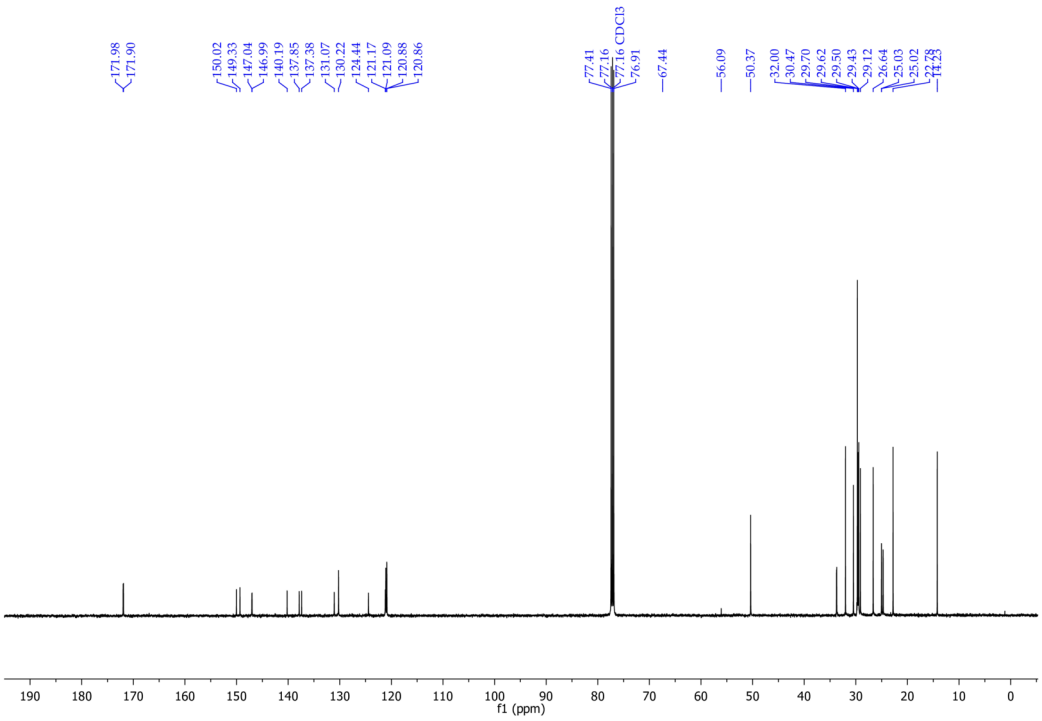

Figure S31. ^{13}C NMR spectrum (125 MHz, $CDCl_3$) of **oP^4(C_{12})**.

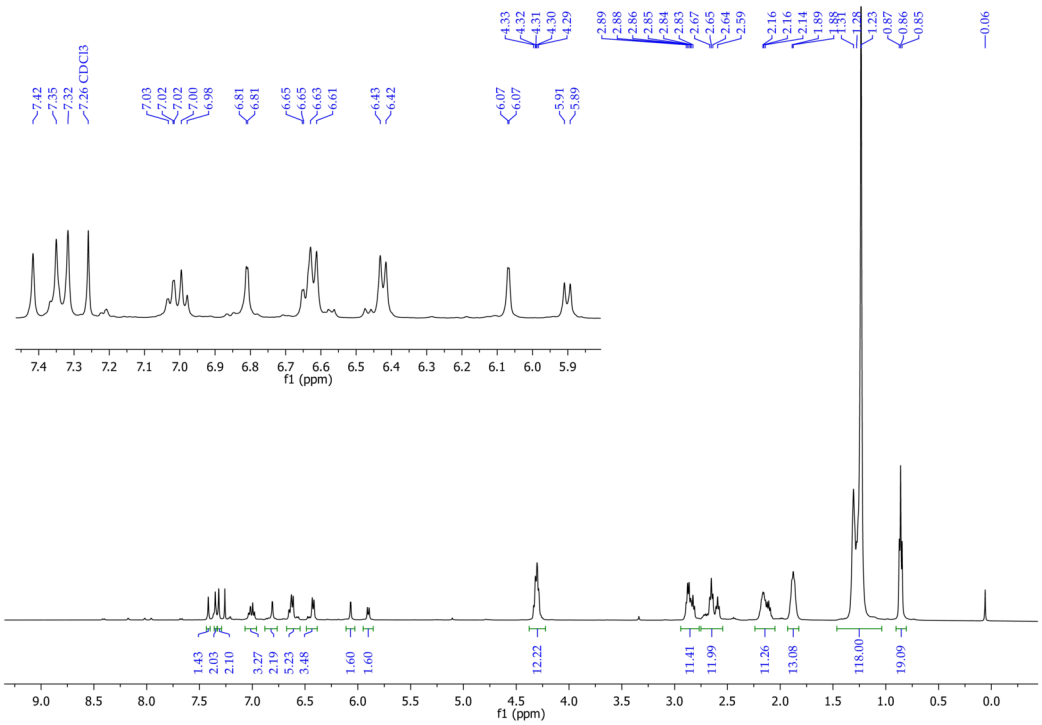

Figure S32. ^{1}H NMR spectrum (500 MHz, $CDCl_3$) of **oP^{6}(C_{12})**.

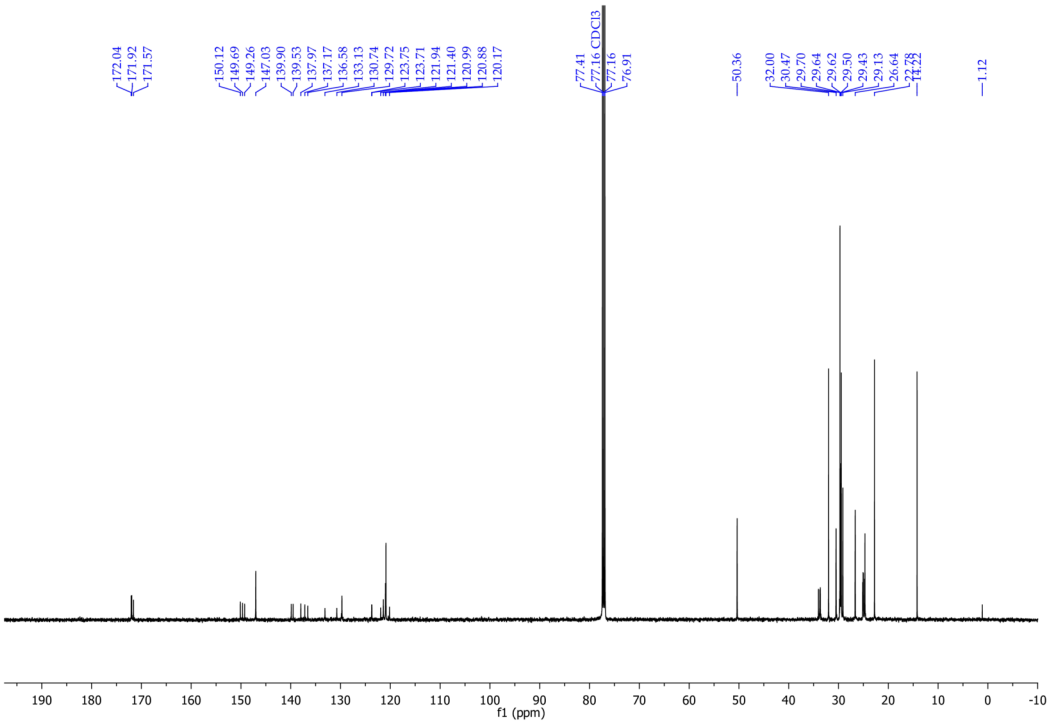

Figure S33. ^{13}C NMR spectrum (125 MHz, $CDCl_3$) of **oP^{6}(C_{12})**.

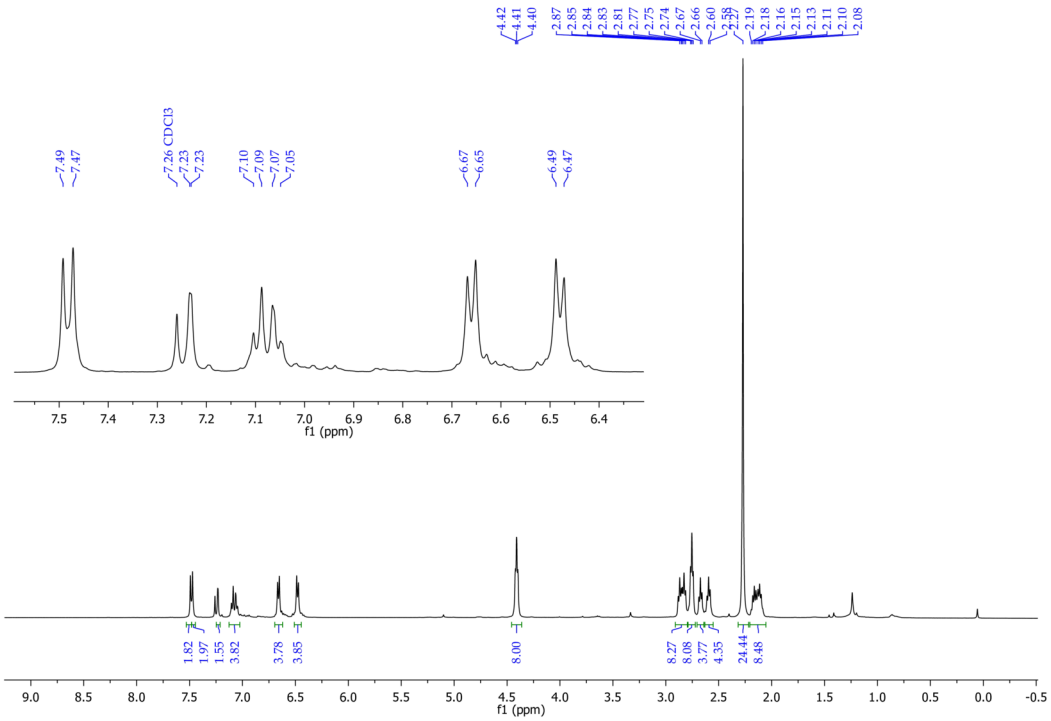

Figure S34. ^{1}H NMR spectrum (500 MHz, $CDCl_3$) of **oP^4(NMe$_2$)**.

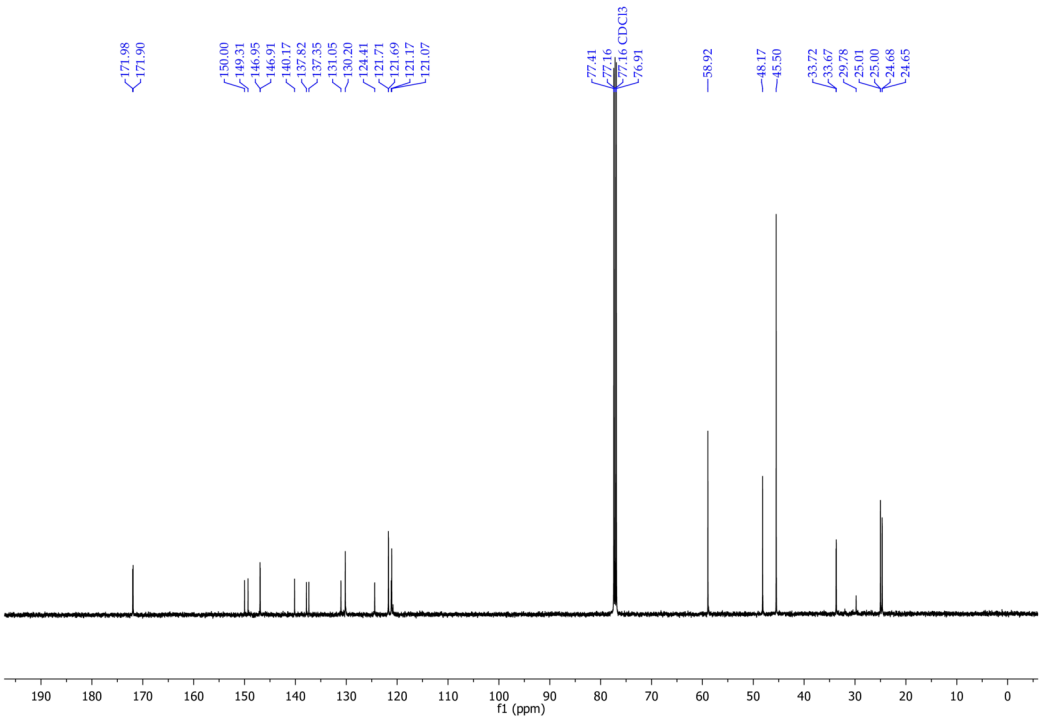

Figure S35. ^{13}C NMR spectrum (125 MHz, $CDCl_3$) of **oP^4(NMe$_2$)**.

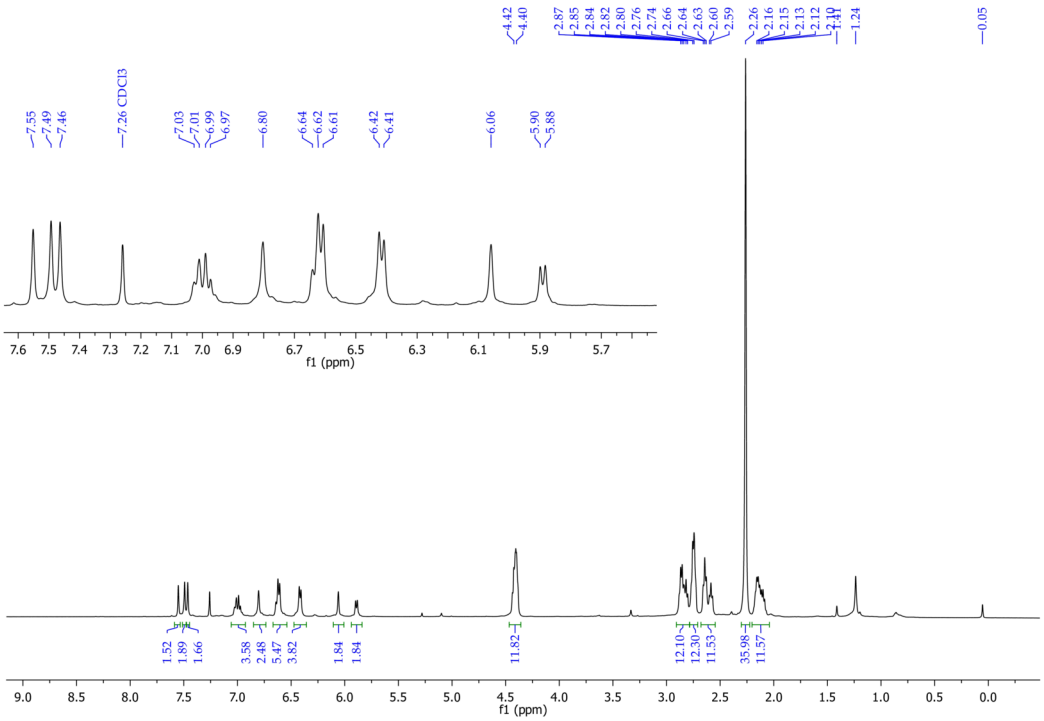

Figure S36. ^{1}H NMR spectrum (500 MHz, $CDCl_3$) of **oP^6(NMe$_2$)**.

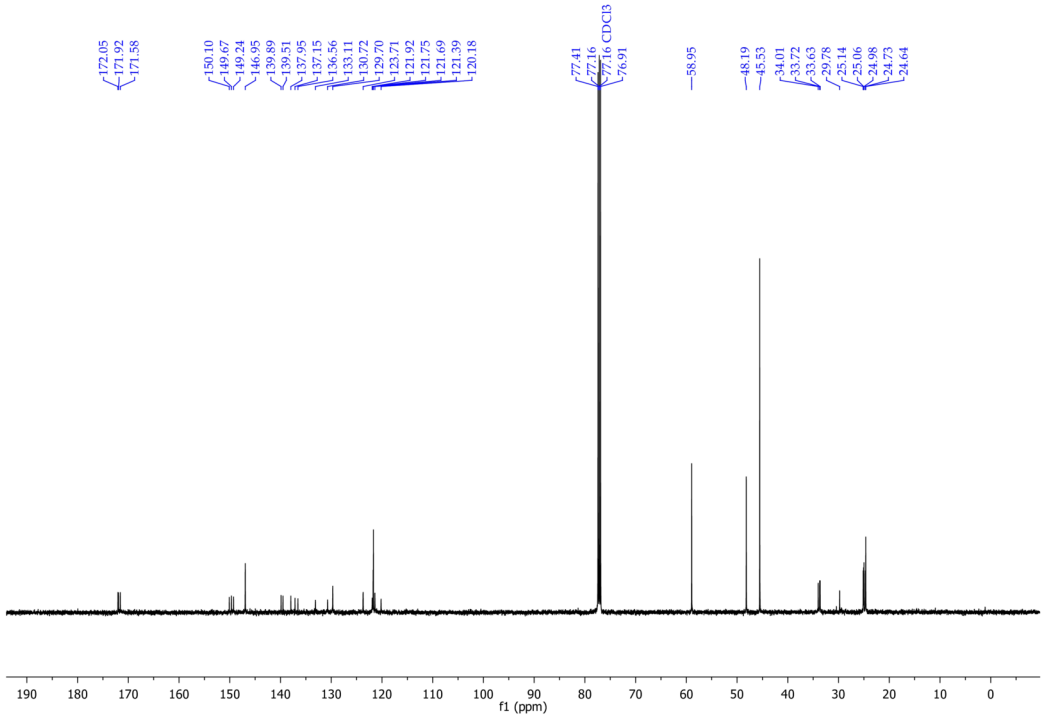

Figure S37. ^{13}C NMR spectrum (125 MHz, $CDCl_3$) of **oP^6(NMe$_2$)**.

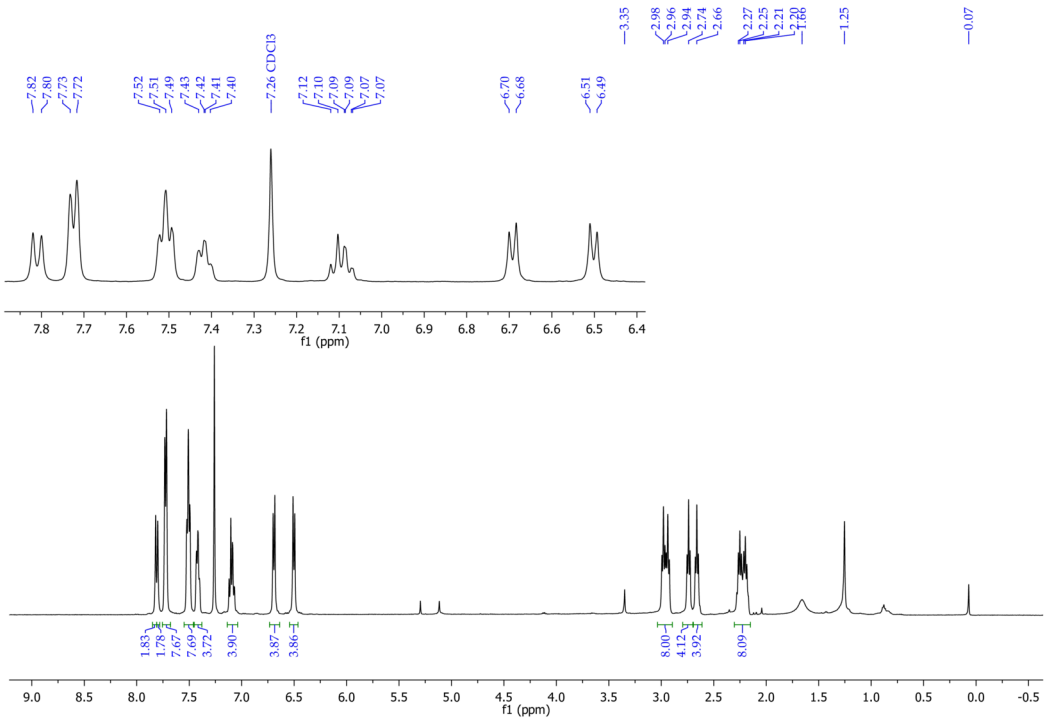

Figure S38. ^{1}H NMR spectrum (500 MHz, $CDCl_3$) of **oP^4(Ph)**.

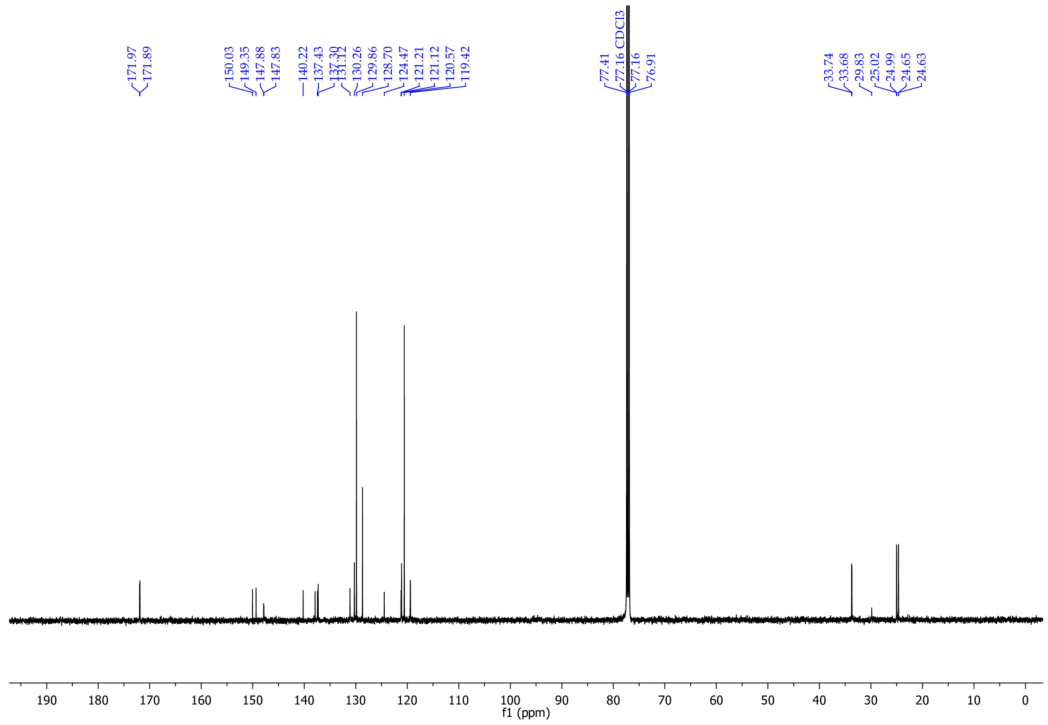

Figure S39. ^{13}C NMR spectrum (125 MHz, $CDCl_3$) of **oP^4(Ph)**.

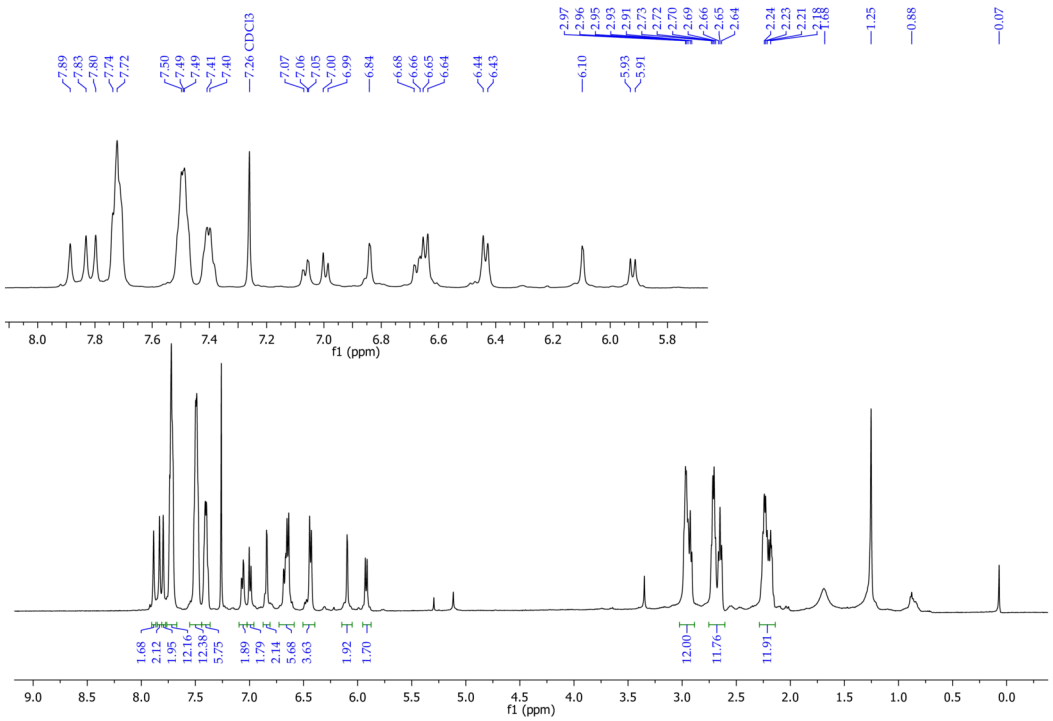

Figure S40. ^{1}H NMR spectrum (500 MHz, $CDCl_3$) of **oP^6(Ph)**.

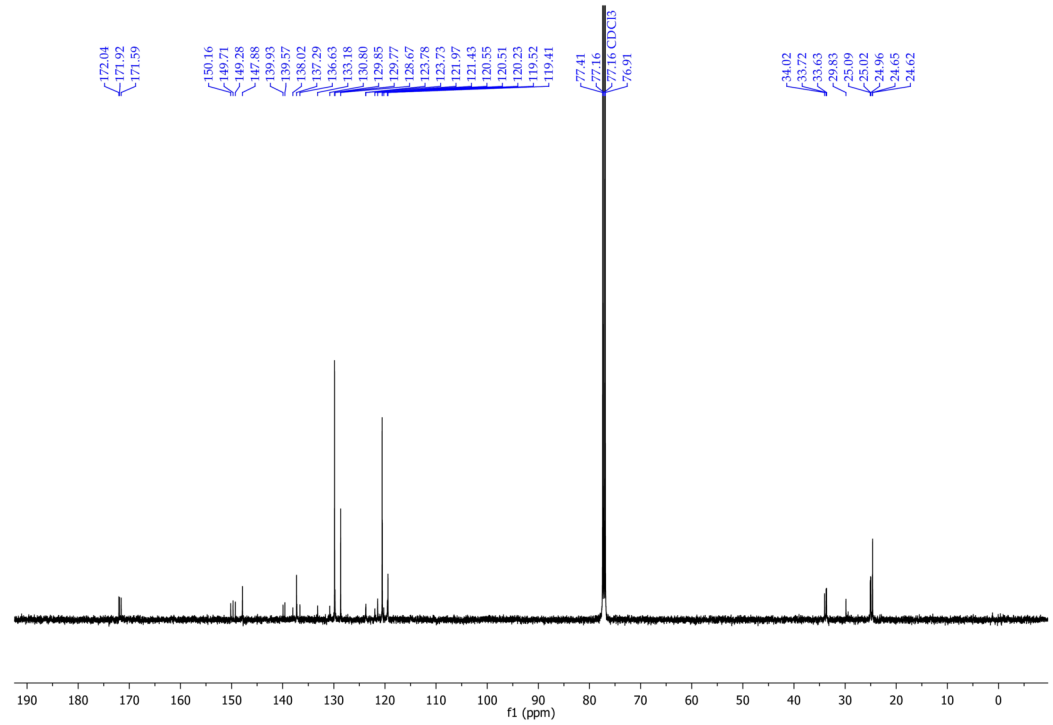

Figure S41. ^{13}C NMR spectrum (125 MHz, $CDCl_3$) of **oP^6(Ph)**.

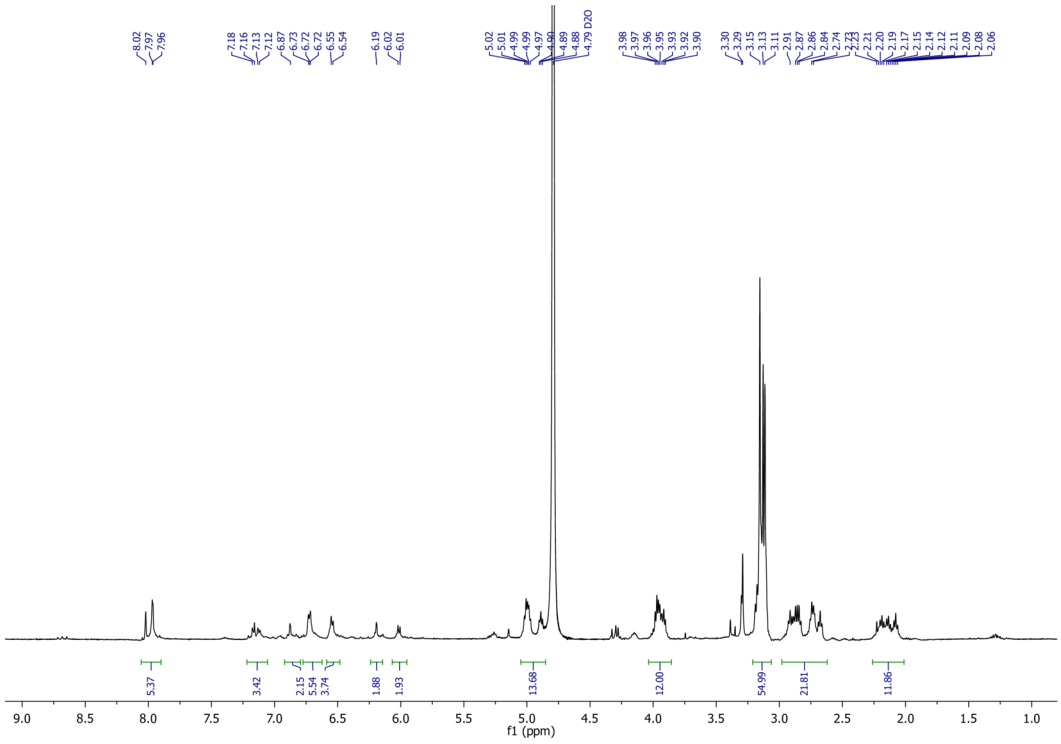

Figure S42. ^{1}H NMR spectrum (500 MHz, D_2O) of **oP^6(NMe$_3^+$)**.

References

(1) C. S. Hartley and J. He, *J. Org. Chem.*, 2010, **75**, 8627–8636.

(2) M. J. Frisch, G. W. Trucks, H. B. Schlegel, G. E. Scuseria, M. A. Robb, J. R. Cheeseman, G. Scalmani, V. Barone, B. Mennucci, G. A. Petersson, H. Nakatsuji, M. Caricato, X. Li, H. P. Hratchian, A. F. Izmaylov, J. Bloino, G. Zheng, J. L. Sonnenberg, M. Hada, M. Ehara, K. Toyota, R. Fukuda, J. Hasegawa, M. Ishida, T. Nakajima, Y. Honda, O. Kitao, H. Nakai, T. Vreven, J. A. Montgomery, Jr, J. E. Peralta, F. Ogliaro, M. Bearpark, J. J. Heyd, E. Brothers, K. N. Kudin, V. N. Staroverov, T. Keith, R. Kobayashi, J. Normand, K. Raghavachari, A. Rendell, J. C. Burant, S. S. Iyengar, J. Tomasi, M. Cossi, N. Rega, J. M. Millam, M. Klene, J. E. Knox, J. B. Cross, V. Bakken, C. Adamo, J. Jaramillo, R. Gomperts, R. E. Stratmann, O. Yazyev, A. J. Austin, R. Cammi, C. Pomelli, J. W. Ochterski, R. L. Martin, K. Morokuma, V. G. Zakrzewski, G. A. Voth, P. Salvador, J. J. Dannenberg, S. Dapprich, A. D. Daniels, O. Farkas, J. B. Foresman, J. V. Ortiz, J. Cioslowski and D. J. Fox, *Gaussian 09, Rev. B.01*, Gaussian, Inc., Wallingford, CT, 2010.

(3) S. Mathew, L. A. Crandall, C. J. Ziegler and C. S. Hartley, *J. Am. Chem. Soc.*, 2014, **136**, 16666–16675.

(4) C. S. Hartley, *Acc. Chem. Res.*, 2016, **49**, 646–654.